Journal of Molecular Graphics and Modelling 126 (2024) 108645

Contents lists available at ScienceDirect

Journal of Molecular Graphics and Modelling

journal homepage: www.elsevier.com/locate/jmgm

The effect of $\{O, N\} = X \cdots M = \{Ti, Zr, Hf\}$ interactions on the sensitivity of C–NO_2 trigger bonds in FOX-7: Approach based on the QTAIM/EDA-NOCV analysis

Nassima Bachir [a], Samir Kenouche [a], Jorge I. Martínez-Araya [b,c,*,1]

[a] Group of Modeling of Chemical Systems using Quantum Calculations, Applied Chemistry Laboratory (LCA). University M. Khider of Biskra, 07000 Biskra, Algeria
[b] Departamento de Ciencias Químicas, Facultad de Ciencias Exactas, Universidad Andres Bello (UNAB), Av. República 275, 8370146 Santiago, Chile
[c] Centro de Química Teórica y Computacional (CQT&C). Facultad de Ciencias Exactas, Santiago, Chile

ARTICLE INFO

Keywords:
Energetic molecules
Sensitivity of trigger bonds
FOX-7 or DADNE
Metallocene methyl cations
ESP/EDA-NOCV/QTAIM analysis

ABSTRACT

The local chemical reactivity of FOX-7 (1,1-diamino-2,2-nitroethylene, also known as DADNE from DiAmino-DiNitroEthylene) was elucidated through a quantitative study of the electrostatic potential on the molecular surface, topological analysis based on Bader's theory, and the EDA-NOCV method. Unlike $(O_2N)_2C{=}C(NH_2){-}H_2\mathbf{N}\cdots Cp_2\mathbf{M}CH_3^+$ complexes, which exhibit both σ-donor and π-acceptor features, the situation is different concerning the $(H_2N)_2C{=}C(NO_2){-}(O)N\mathbf{O}\cdots Cp_2\mathbf{M}CH_3^+$ complexes, where both charge transfers correspond to the σ-donation. The two charge transfers reinforce each other, resulting in increased stability for $(H_2N)_2C{=}C(NO_2){-}(O)N\mathbf{O}\cdots Cp_2\ \mathbf{M}CH_3^+$. This seems to strengthen the $(H_2N)_2C{=}C(NO_2){-}(O)N\mathbf{O}\cdots M{=}\{Ti, Zr, Hf\}$ bond, which may explain the high stability of $(H_2N)_2C{=}C(NO_2){-}(O)N\mathbf{O}\cdots Cp_2\mathbf{M}CH_3^+$ compared to $(O_2N)_2C{=}C(NH_2){-}H_2\mathbf{N}\cdots Cp_2\mathbf{M}CH_3^+$. Results from topological analysis revealed that the decreased sensitivity to decomposition of C–NO_2 bonds depends on the chemical nature of the interacting metal, and the best achievements are obtained for the Hf-based complex. Our results demonstrate that the interaction of $M = \{Ti, Zr, Hf\}$ with C–NO_2 is more favourable than that with C–NH_2, this specific action on the trigger bond may support the use of Metallocene Methyl Cations (MMC) as possible neutralisers.

1. Introduction

Understanding the decomposition process is an increasingly crucial factor in the field of energetic materials (EM) [1–3]. The trigger bond, also known as the "trigger linkage mechanism", is a widely accepted concept in the decomposition mechanism of such materials [4–9]. This concept was first defined by Kamlet and Adolph [10], and allows to understand the impact sensitivity of EM from a molecular perspective. The trigger bond is a concept referred to as the trend presented by certain bonds to break apart in EM as a response to energy input from an external stimulus; their rupture "triggers" the exothermic decomposition that characterises detonation [11]. Sensitivity to detonation is an essential characteristic of EM. This property refers to the vulnerability of these compounds to unexpected detonation due to an involuntary stimulus (sparks, friction, shock, etc.) [12–14]. An explosion caused by these molecules occurs when a highly exothermic reaction takes place, instantly releasing a large amount of heat along with a large amount of gas, which expands and moves at high speed [15,16]. One of the main challenges in EM is reducing the sensitivity without losing the detonation efficiency, although these two objectives seem intrinsically contradictory. From a practical point of view, an optimal balance between these two fundamental characteristics achieves this task. Other essential facts, such as cost of synthesis and transformability are considered for designing new energetic molecules.

Non-explosive reaction channels for the decomposition of EM have been proposed [11,17,18], which could be attained by selecting specific chemical compounds to react on certain sites of an energetic molecule, and preventing the latter from following its normal explosion channel. The surfaces of EM are prone to possessing quite positive electrostatic potentials [19], suggesting reactivity towards nucleophiles. It is a well known fact that nitroaromatics react with amines [20]. The 2,4,6-trinitrotoluene (TNT) can be neutralised by exposure to aliphatic amines, leading to hypergolic combustion of the TNT [21]. In this study, we define a neutraliser as a molecule able to form a complex with an energetic molecule, thus preventing the latter from following its

* Corresponding author at: Departamento de Ciencias Químicas, Facultad de Ciencias Exactas, Universidad Andres Bello (UNAB), Av. República 275, 8370146 Santiago, Chile.
E-mail address: jorge.martinez@unab.cl (J.I. Martínez-Araya).
[1] Present address: Av. República 275, Santiago-Chile.

https://doi.org/10.1016/j.jmgm.2023.108645
Received 28 March 2023; Received in revised form 27 September 2023; Accepted 27 September 2023
Available online 4 October 2023
1093-3263/© 2023 Published by Elsevier Inc.

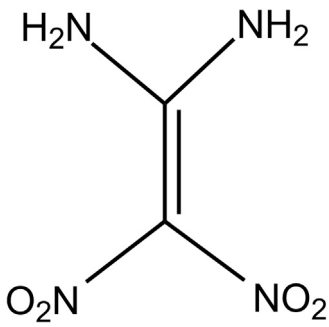


Fig. 1. Structural formula of FOX-7, also known as DADNE.

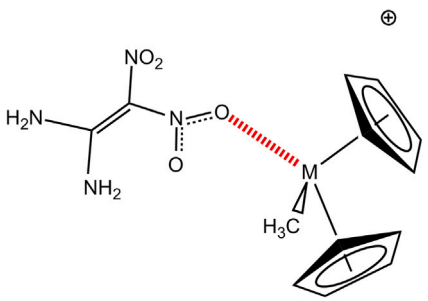


Fig. 2. Interaction **O**···**M** leading to the complex of type $(H_2N)_2C{=}C(NO_2)$-(O)N**O**···Cp_2**M**CH_3^+.

explosive reaction channel. To this end, we are looking to stabilise the C-NO_2 trigger bond in FOX-7 (1,1-diamino-2,2-nitroethylene, Fig. 1) through intermolecular interactions involving group IV transition metals (M = {Ti, Zr, Hf}) in metallocene methyl cations (MMC). FOX-7 is an energetic molecule first synthesised in 1998 by Latypov et al. [22].

Despite its simple composition and structure, its chemical reactivity is extremely rich [23]. This molecule has attracted an increasing interest in many theoretical and experimental investigations [24–29]. More precisely, many studies have highlighted the decomposition mechanism of FOX-7 using different experimental and theoretical methods, and there is evidence that breaking C-NO_2 bonds is a crucial step in the initiation of decomposition [30–34].

Some polymerisation processes use MMC for their catalytic properties exerted on π-electron bearing monomers through the Cossè–Arlman mechanism [35,36] which can be explained by mean of a coordination of these monomers on metallic centre of the MMC. The aim of this work is to use the coordination capability of the MMC to prevent the explosion channel. FOX-7 can interact with MMC through its nucleophilic regions (lone pair electrons of NO_2) according to an electrophilic addition reaction. The nitrogen atom of NO_2 can interact with a nucleophilic moiety from MMC because this atom is positively charged. The formation of such complexes can enhance the trigger bond strength. Therefore, the sensitivity of the EM decreases.

In a previous study [37], we have already shown the effectiveness of MMC in reducing the sensitivity of the N-NO_2 trigger bonds in cyclic energetic compounds, where the only type of interplay between HMX (1,3,5,7-Tetranitro-1,3,5,7-tetrazocane)/RDX (1,3,5-trinitro-1,3,5-triazine) and MMC involves Oxygen···metal interaction. At the present work, we detected two possible interactions which deserved a more detailed analysis: Oxygen···metal and Nitrogen···metal. The former is the expected one and the latter is the non expected one. We needed to address both types of interactions in order to discard the weakest one and use the strongest one thus providing a support for the FOX-7 and MMC interplay. We had the preliminary hypothesis that Nitrogen···metal interaction was as important as Oxygen···metal interaction found when HMX (or RDX) and MMC interplays one each other. Moreover, reducing the sensitivity of FOX-7 is challenging, as this molecule is known for its low sensitivity compared to the cyclic compounds [38,39]. Besides, the FOX-7 molecule is interesting because it also contains two C-NH_2 bonds that are not trigger bonds and, hence, are not directly involved in the explosion process. Indeed, the bond dissociation energies have been evaluated by 293 kJ/mol for C-NO_2 and by 466 kJ/mol for C-NH_2, therefore the former is more unstable and breaks more easily in detonation initiation [40]. These dissociation energy values change with the number of NO_2 linked to the carbon [41]. The NH_2 group generates both inductive and resonance effects. The nitrogen atom being more electronegative than the carbon, tends to pull out electrons from the carbon–carbon double bond by inductive effect, and it can also provide its lone pair through a resonance effect. The aim is to study the influence of these effects on the C-NO_2 bonds before and after forming the complexes. This analysis is crucial to validate the proposal of using MMC as a neutraliser of energetic molecules by forming a complex because finding a pattern of interaction we could suggest the use of MMC to neutralise or at least deviate the typical behaviour of an energetic molecule to follow a safe reaction channel not leading to an explosive decomposition.

In addition, an experimental evidence revealed a link between the presence of NH_2 groups and the sensitivity of EM [19]. This fact is probably owing to molecules in which electron delocalisation is possible. NH_2, known as an electron donating group by resonance, is able to partially or totally compensate the potential imbalance created by the electron-withdrawing NO_2 groups. This compensating effect depends on the number of NH_2 groups included in the energetic molecule. Besides, a network of intramolecular hydrogen bonds may enhance the stability of such molecules [42]. The effect of NH_2 groups on sensitivity may also be caused by all these factors at once [43]. In this study, we examined three types of interactions: oxygen and nitrogen from a nitro group interacting with the metal atom, as well as nitrogen from an amino group interacting with the metal atom. Furthermore, we also analysed the effect of NH_2 groups on the sensitivity of the C-NO_2 trigger bond in FOX-7.

The topological analysis and the decomposition of intermolecular interaction energies between the two molecular fragments were conducted using QTAIM (Quantum Theory of Atoms in Molecules) and EDA-NOCV (Energy Decomposition Analysis with Natural Orbitals for Chemical Valence) methods, respectively. The EDA-NOCV approach unlike most other energy decomposition methods focuses on the mechanism of bond formation between the interacting molecular fragments and not just only on the analysis of the finally formed bonding [44]. This method also provides an effective way through the study of deformation densities to quantitatively assess the σ-donor and π-acceptor properties of MMC. The QTAIM topological approach was performed to elucidate the nature of the different interactions involved in complexes $(H_2N)_2C{=}C(NO_2)$-(O)N**O**···Cp_2**M**CH_3^+ (Fig. 2) and $(O_2N)_2C{=}C(NH_2)$-H_2**N**···Cp_2**M**CH_3^+, in which the interacting atoms are highlighted in bold (Fig. 3). The chemical reactivity of FOX-7 towards nucleophilic and electrophilic reagents was elucidated through the electrostatic potential on the molecular surface [45–48].

This scalar field is regularly employed to assess the sensitivity of EM to detonation, especially concerning the electron density depletion in the central regions of the molecular surface [49–52]. In addition, some of statistically-based indices [53–55] derived from molecular surface electrostatic potentials were discussed. The present work is understood within the framework of ionic chemistry in the gas phase which is supported by the investigation performed by Mó and Yáñez [56–58].

1.1. Theoretical framework of EDA-NOCV

The EDA-NOCV is a very popular method used to analyse in depth qualitatively and quantitatively the nature of chemical bonds between

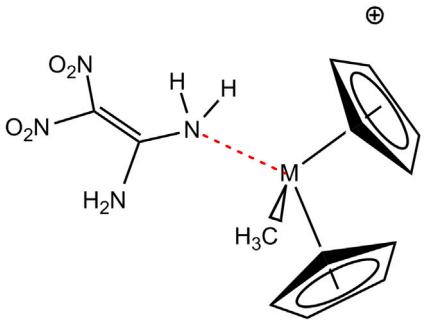


Fig. 3. Interaction **N**···**M** leading to the complex of type $(O_2N)_2C{=}C(NH_2)$-$H_2\mathbf{N}\cdots Cp_2\mathbf{M}CH_3^+$.

interacting molecular fragments [59–62]. This method combines the energy decomposition analysis proposed by Ziegler and Rauk [63,64], with the NOCV concept described by Mitoraj and Michalak [65,66]. In this approach, the interaction energy (ΔE_{int}) is primarily divided into three physically meaningful terms. The dispersion interaction (ΔE_{disp}) arises from an explicit correction associated with D3BJ functional. In this way, a fourth extra contribution is added to the interaction energy equation according to:

$$\Delta E_{int} = \Delta E_{Pauli} + \Delta E_{orb} + \Delta E_{elstat} + \Delta E_{disp} \tag{1}$$

The orbital interaction (ΔE_{orb}) accounts for charge, polarisation, and electron-pair bonding [67]. This term reflects the energy involved in the bond formation, which yields a relevant description of the bonding situation in the equilibrium geometry [68,69].

ΔE_{Pauli} represents the repulsive interaction between electrons with the same spin due to Pauli principle, which is also called exchange-repulsion term. ΔE_{elstat} is the classical electrostatic interaction between the molecular fragments. Within the theoretical framework of EDA-NOCV, the ΔE_{orb} may be separated into contributions associated with the NOCV pairs according to:

$$\Delta E_{orb} = \sum_{i=1}^{N} \Delta E_{orb}^{(i)} = \sum_{i=1}^{N/2} \nu_i \left[F_{i,i}^{TS} - F_{-i,-i}^{TS}\right] \tag{2}$$

where i is an index of NOCV, $F_{i,i}^{TS}$ and $F_{-i,-i}^{TS}$ are the ith diagonal terms of transition-state Kohn–Sham matrix elements corresponding to NOCV with the eigenvalues ν_i and ν_{-i}, respectively. The key feature of this analysis is its ability to deconvolute variation of electron density due to orbital interaction to a set of NOCV pairs $\{\phi_i(\mathbf{r}), \phi_{-i}(\mathbf{r})\}$ of complementary orbitals with the same eigenvalue and opposite sign as shown by:

$$\Delta\rho(\mathbf{r}) = \sum_{i=1}^{N/2} \Delta\rho_{(i)}^{orb}(\mathbf{r}) = \sum_{i=1}^{N/2} [\nu_i \phi_i^2(\mathbf{r}) + \nu_{-i} \phi_{-i}^2(\mathbf{r})] \tag{3}$$

Each two NOCV orbitals with opposite eigenvalues constitute a NOCV pair. The Eq. (3) allows us to quantify the amount of electron density transferred between fragments. There are frequently many NOCV orbitals, among which only a few pairs have significant effect on the deformation density, $\Delta\rho(\mathbf{r})$. NOCV pairs with a larger eigenvalue magnitude show a more significant effect on the deformation density caused by the orbital interaction. For this reason, usually only the first two NOCV pairs are considered.

2. Computational detail

All molecular structures were fully optimised using Gaussian16 Revision B.01 [70]. We employed the CAM-B3LYP [71] and ωB97X-D [72] exchange–correlation functionals along with the following effective core potentials: MDF10, MWB28, MWB60 for Ti, Zr, and Hf, respectively [73]. The O, N, C, and H atoms were represented using the 6-31+G(d,p) basis set. The atomic coordinates of the six complexes obtained with the CAM-B3LYP and ωB97X-D density functionals are included in ESI (Electronic Supporting Information). The EDA-NOCV method was carried out by single-point calculations on the optimised structures employing the Amsterdam Density Functional software (ADF 2013.01) [74] using the revPBE-D3BJ functional. This density functional combines the revised Perdew–Burke–Ernzerhof exchange–correlation (revPBE) [75] with the D3BJ dispersion correction [76]. Goerigk et al. [77] recommend the use of revPBE-D3BJ for its ability to efficiently describe non-covalent interactions. A Slater type orbital (STO) basis set [78] of triple zeta quality with two polarisation functions (TZ2P) was considered for all atoms using Becke integration grid [79] of "very good" precision and without a frozen core. Scalar relativistic effects were included through the zero-order regular approximation (ZORA) [80]. The cube files produced by ADF software were used to visualise the deformation densities isosurfaces by using Visual Molecular Dynamics (VMD) program [81]. The electrostatic potential on the molecular surface as well as the topological analysis were conducted using the Multiwfn 3.8 code [82] based on the formatted Gaussian checkpoint file. To ensure the reproducibility of the results, all the calculations (QTAIM and EDA-NOCV) in this study were performed on the molecular structures optimised by the CAM-B3LYP and ωB97X-D density functionals (see Tables S1 to S4 in ESI). Further, the interaction energy is also calculated using various density functionals from a single point calculation (see Table S5 in ESI). The chemical structures of all the compounds are depicted in Figure S1 (see ESI).

3. Results and discussion

3.1. Electrostatic potential analysis

For predicting the reactivity of a molecule towards an approaching reactant, one typically plots the electrostatic potential (ESP) on a van der Waals surface of the molecule of $\rho(\mathbf{r}) = 0.001\,\mathrm{e/Bohr}^3 \equiv$ a.u, which covers about 98% of the negative charge. This isosurface value was proposed by R. Bader [83], which reflects specific electron structure features of a molecule, such as π-electrons and lone pairs of heteroatoms. The ESP measures the electrostatic interaction between a unit point charge placed at **r** and the molecule of interest. Negative and positive values indicate that current position is dominated by electronic and nuclear charges, respectively. The reactive site closer to the global ESP maximum (minimum) on van der Waals surface is theoretically the most electrophilic (nucleophilic) site. The mapped-ESP onto a surface of constant electron density surrounding FOX-7 along with the surface extrema are shown in Fig. 4. As can be seen, the positive ESP values are around the NH_2 groups, reflecting the electrostatic repulsion between the unit charge (a proton) and the atomic nuclei.

These regions are characterised by low electron density, where the nuclear charge is partially shielded. The absence of an electron-rich site in NH_2, proves that the nitrogen lone pair is involved in a resonance structure. As expected, we observe strongly negative peripheral regions around the NO_2 groups. These electron-rich sites are mainly attributable to the lone pairs of oxygen atoms. The positive ESP values above the C-NO_2 bonds indicate a decrease in electron density due to the high electron-withdrawing effect of NO_2, leading to a weakening of these bonds.

The regions coloured in shades of white, which are electrically neutral, reflect the transition area between positively and negatively charged regions. The global maximum ($V_{s,max}$) on the potential surface with a value of 73.35 kcal/mol is reached in the region between the two amino groups. On the other hand, its global minimum ($V_{s,min}$) with a value of −38.24 kcal/mol is located between the two nitro groups. The global maximum reflects the most electron-deficient site, susceptible to easily undergoing a nucleophilic attack, while the global minimum refers to the most electron-rich site, which preferentially attracts electrophilic reagents. This charge separation induces a polarisation along

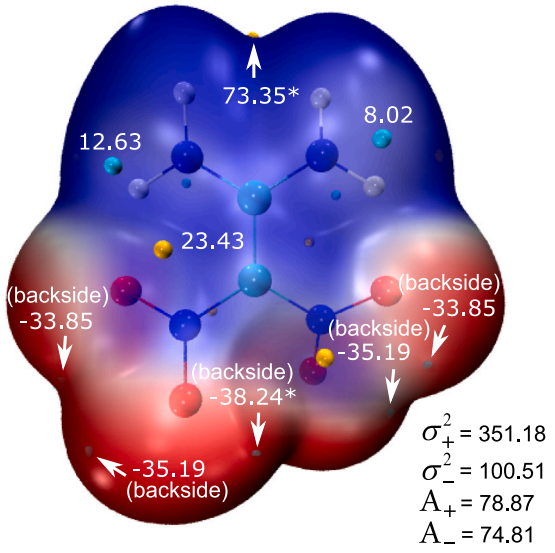


Fig. 4. ESP-mapped van der Waals surface (kcal/mol) using a colour scale ranging from red (negative ESP), through white (neutral ESP) to blue (positive ESP). The blue regions are prone to nucleophilic attack, and the red regions are sites for electrophilic attack. The grid spacings were set to 0.2 Bohr and the van der Waals surface denotes the iso-surface of $\rho = 0.001\,\mathrm{e/Bohr^3} \equiv 0.001$ a.u. Values with a star indicate global surface extreme. The bold numbers in the bottom right-hand corner are the positive ESP variance (σ^2_+), negative ESP variance (σ^2_-), positive surface area (A_+) and negative surface area ($A_$) whose units are (Kcal/mol)^2 Å^2, respectively. (For interpretation of the references to colour in this figure legend, the reader is referred to the web version of this article.)

the central axis passing through the two carbons. As reported by Zhang et al. [23], the positive end of the carbon–carbon double bond can undergo nucleophilic attack. The pattern of the surface potential reveals an imbalance in the total charge distribution induced by the two electron-donating amino groups and the two electron-accepting nitro groups. Indeed, the nitro groups tend to decrease the electron density over the carbon–carbon double bond. In contrast, the amino groups tend to enhance the electron density above the carbon–carbon double bond.

These two antagonistic effects give rise to the so-called push–pull effect [40]. The depletion of electron density around the carbon–carbon double bond also indicates that electron-withdrawing NO_2 groups predominate over electron-donating NH_2 groups. The positive (A_+) and negative ($A_$) surface areas are slightly different, with respective contributions of 51.4% and 48.6% to the total area. The positive (σ^2_+) and negative (σ^2_-) variance contributions are 77.7% and 22.3% compared to the total variance, respectively. The $\sigma^2_+ > \sigma^2_-$ suggests a strong positive charge density fluctuation compared to the negative charge density. This result is typical of energetic molecules characterised by a strong concentrated positive charge in the central regions, in contrast to the negative charges spread in the peripheral regions. FOX-7 shows a tendency to react preferentially as an electrophilic entity. It is worth noting that for most organic molecules $\sigma^2_- > \sigma^2_+$, since the positive regions come mainly from hydrogen atoms and the negative regions are dominant, such as lone pairs of heteroatoms and π-electrons in aromatic systems and multiple bonds [84].

3.2. Topological analysis of electron density

The Bader's theory [85,86] was used to quantitatively analyse the chemical nature of the $\{O,N\} = X\cdots M = \{Ti,Zr,Hf\}$ bonding. Some theoretical details on this theory are given in ESI. The molecular graphs of $(H_2N)_2C{=}C(NO_2)$-(O)N**O**$\cdots Cp_2$**M**CH_3^+ and $(O_2N)_2C{=}C(NH_2)$-H_2**N**$\cdots Cp_2$**M**CH_3^+ are depicted in Figures S2 and S3 (see ESI), respectively. The numerical values calculated at the bond critical points (BCPs) are quoted in Tables 1 and 2. As can be seen from Figures S2 and S3, the presence of a bonding path (line of maximum density) between $\{O,N\} = X$ and $M = \{Ti,Zr,Hf\}$ means that these atoms are linked by an interaction. From QTAIM's point of view, the formation of a (3, −1) saddle point associated with its bonding path satisfies both necessary and sufficient conditions of negative charges accumulation in the interatomic region [87,88].

The electron density is the first parameter that emerges when investigating the nature and strength of chemical bonds. The more C-NO_2 bonds are deficient in electron density, the weaker these bonds and therefore it becomes easy to break them to initiate the detonation process. From Table 1, the electron densities obtained at the BCPs vary from 0.041 to 0.045 e Å^{-3} for $N\cdots M = \{Ti,Zr,Hf\}$ and from 0.058 to 0.062 e Å^{-3} for $O\cdots M = \{Ti,Zr,Hf\}$, indicating that the latter is stronger. The values of $\nabla^2\rho(\mathbf{r_B})$ are all positive, revealing an electron density depletion in the interatomic region, and therefore the $\{O,N\} = X\cdots M = \{Ti,Zr,Hf\}$ bonding seems to belongs to the closed-shell type. The total energy density $H(\mathbf{r_B})$ at the BCP is a very meaningful index to characterise the nature of interactions, which is used in many QTAIM investigations involving both strongly and weakly interacting complexes [89–91]. A negative value of $H(\mathbf{r_B})$ is evidence of a covalent pairwise atom–atom interaction [92]. The $H(\mathbf{r_B})$ values are all positive and close to zero, except in the case of N···Ti, where $H(\mathbf{r_B})$ is negative which can be considered as an indicator of covalency. This means that $V(\mathbf{r_B})$ and $G(\mathbf{r_B})$ contribute locally with similar values in all complexes while $V(\mathbf{r_B})$ slightly dominates in $(O_2N)_2C{=}C(NH_2)$-H_2**N**$\cdots Cp_2$**Ti**CH_3^+. The $|V(\mathbf{r_B})|/G(\mathbf{r_B})$ ratio at the BCP may be construed as a measure of covalent character of an interaction [92].

This ratio is very informative in this regard, since some authors [93] point out that $1 < |V(\mathbf{r_B})|/G(\mathbf{r_B}) < 1.10$ is typical of an ionic bond with a partially covalent character, and thus the N···Ti bonding can be classified in this category.

As expected, in Table 2 we can see that the C-NH_2 bond is stronger as compared to C-NO_2. The nitrogen atom is positively charged in NO_2 group and negatively charged in NH_2 group, since the carbons are positively charged in both C-NO_2 and C-NH_2, from a purely electrostatic point of view, the C-NO_2 bond which is repulsive in nature is weaker than the C-NH_2 bond that is attractive.

Therefore, the sensitivity to detonation is higher for the C-NO_2 bond. The sensitivity of the C-NO_2 bond was quantified by calculating some topological parameters at the BCP before and after the complex's formation. The possible deactivation of this bond is determined by evaluating the difference in topological parameters for the same C-NO_2 in the isolated compound ($X(\mathbf{r_B})^0$) and in the complex ($X(\mathbf{r_B})^{\#}$) according to [61]:

$$\Delta X(\mathbf{r_B}) = \frac{X(\mathbf{r_B})^{\#} - X(\mathbf{r_B})^0}{X(\mathbf{r_B})^0} \tag{4}$$

where $\Delta X(r_B)$ represents the difference in the topological property ($\rho(r_B)$ or $H(r_B)$), $X(r_B)^{\#}$ and $X(r_B)^0$ denote the property calculated at the BCP in the complex and the isolated molecule, respectively.

In this way, the influence of $\{O,N\} = X\cdots M = \{Ti,Zr,Hf\}$ intermolecular interactions on the C-NO_2 bond can be evaluated. In this respect, Eq. (4) is applied to $\rho(\mathbf{r_B})$ and $H(\mathbf{r_B})$. The numerical values obtained are highlighted in bold in Table 2.

In complexes $(H_2N)_2C{=}C(NO_2)$-(O)N**O**$\cdots Cp_2$**M**CH_3^+, the electron density at the BCP of C-NO_2 increases, where the largest percentage (8.4%) was obtained for both $(H_2N)_2C{=}C(NO_2)$-(O)N**O**$\cdots Cp_2$**Zr**CH_3^+ and $(H_2N)_2C{=}C(NO_2)$-(O)N**O**$\cdots Cp_2$**Hf**CH_3^+. A similar trend with higher percentages (from 19.3 to 21.5%) is obtained for the property $H(\mathbf{r_B})$. The C-NO_2 bond is affected by the interaction between the oxygen atom from nitro group and the transition metal. This strengthening enhances the structural stability towards decomposition, especially for the Hf- and Zr-based complexes.

A completely opposite pattern is observed in complexes $(O_2N)_2C{=}C(NH_2)$-H_2**N**$\cdots Cp_2$**M**CH_3^+, for which both $\rho(\mathbf{r_B})$ and $H(\mathbf{r_B})$ decrease after

Table 1
Topological properties of the electron density calculated at the (3, −1) bond critical point for the {O, N} = X ⋯ M = {Ti, Zr, Hf} bonding at DFT/CAM-B3LYP level of theory. The vector $\mathbf{r_B}$ locates the position of the critical point.

Bond	dist.[a]	$\rho(\mathbf{r}_B)^b$	$\nabla^2\rho(\mathbf{r}_B)^c$	$H(\mathbf{r}_B)^d$	$V(\mathbf{r}_B)^e$	$G(\mathbf{r}_B)^f$	$-V(\mathbf{r}_B)/G(\mathbf{r}_B)$
			$(O_2N)_2C{=}C(NH_2)\text{-}H_2N{\cdots}Cp_2MCH_3^+$				
Ti31⋯N30	2.3060	0.0426	0.1292	−0.0027	−0.0378	0.0351	1.0769
Zr31⋯N30	2.4512	0.0418	0.1507	0.0008	−0.0359	0.0367	0.9782
Hf31⋯N30	2.4055	0.0453	0.1663	0.0002	−0.0369	0.0371	0.9946
			$(H_2N)_2C{=}C(NO_2)\text{-}(O)NO{\cdots}Cp_2MCH_3^+$				
Ti39⋯O37	2.1002	0.0625	0.2990	0.0001	−0.0744	0.0746	0.9973
Zr39⋯O37	2.2255	0.0580	0.3005	0.0041	−0.0667	0.0709	0.9407
Hf39⋯O37	2.2050	0.0622	0.3383	0.0042	−0.0680	0.0722	0.9418

[a]Bond distance (Å), [b]Electron density (e Å^{-3}), [c]Laplacian of the electron density (e Å^{-5}), [d]Total electron energy density ($Hartree$ Å^{-3}), [e]Potential electron energy density ($V(\mathbf{r}_B)$, $Hartree$ Å^{-3}), [f]Kinetic electron energy density ($G(\mathbf{r}_B)$, $Hartree$ Å^{-3}).

Table 2
Topological properties of the electron density calculated at the (3, −1) bond critical point of the C-NO_2 and C-NH_2 bonds at the DFT/CAM-B3LYP level of theory. bonding at DFT/CAM-B3LYP level of theory.

Compound	Bond	dist.[a]	$\rho(\mathbf{r}_B)^b$	$\nabla^2\rho(\mathbf{r}_B)^c$	$H(\mathbf{r}_B)^d$	$V(\mathbf{r}_B)^e$	$G(\mathbf{r}_B)^f$	$-V(\mathbf{r}_B)/G(\mathbf{r}_B)$
			C-NO_2 bond					
FOX-7	C2-N10	1.425	0.286	−0.790	−0.409	−0.620	0.211	2.934
$(H_2N)_2C{=}C(NO_2)\text{-}(O)NO{\cdots}Cp_2TiCH_3^+$	C26-N34	1.373	0.305 (**6.6%**)[g]	−0.363	−0.488 (**19.3%**)[g]	−0.886	0.397	2.228
$(H_2N)_2C{=}C(NO_2)\text{-}(O)NO{\cdots}Cp_2ZrCH_3^+$	C26-N34	1.366	0.309 (**8.0%**)[g]	−0.326	−0.495 (**21.0%**)[g]	−0.910	0.414	2.197
$(H_2N)_2C{=}C(NO_2)\text{-}(O)NO{\cdots}Cp_2HfCH_3^+$	C26-N34	1.364	0.310 (**8.4%**)[g]	−0.312	−0.497 (**21.5%**)[g]	−0.917	0.419	2.186
$(O_2N)_2C{=}C(NH_2)\text{-}H_2N{\cdots}Cp_2TiCH_3^+$	C25-N27	1.448	0.280 (**−2.1%**)[g]	−0.834	−0.360 (**−11.9%**)[g]	−0.513	0.152	3.369
$(O_2N)_2C{=}C(NH_2)\text{-}H_2N{\cdots}Cp_2ZrCH_3^+$	C25-N27	1.443	0.282 (**−1.4%**)[g]	−0.842	−0.367 (**−10.3%**)[g]	−0.524	0.1566	3.3461
$(O_2N)_2C{=}C(NH_2)\text{-}H_2N{\cdots}Cp_2HfCH_3^+$	C25-N27	1.448	0.280 (**−2.1%**)[g]	−0.835	−0.359 (**−12.2%**)[g]	−0.509	0.150	3.391
			C-NH_2 bond					
FOX-7	C1-N3	1.339	0.344	−1.185	−0.553	−0.810	0.257	3.152
$(H_2N)_2C{=}C(NO_2)\text{-}(O)NO{\cdots}Cp_2TiCH_3^+$	C25-N30	1.330	0.349 (**1.4%**)[g]	−1.090	−0.582 (**5.2%**)[g]	−0.892	0.310	2.879
$(H_2N)_2C{=}C(NO_2)\text{-}(O)NO{\cdots}Cp_2ZrCH_3^+$	C25-N30	1.328	0.350 (**1.7%**)[g]	−1.086	−0.584 (**5.6%**)[g]	−0.898	0.313	2.867
$(H_2N)_2C{=}C(NO_2)\text{-}(O)NO{\cdots}Cp_2HfCH_3^+$	C25-N30	1.328	0.350 (**1.7%**)[g]	−1.085	−0.585 (**5.7%**)[g]	−0.899	0.314	2.864
$(O_2N)_2C{=}C(NH_2)\text{-}H_2N{\cdots}Cp_2TiCH_3^+$	C26-N30	1.413	0.304 (**−11.6%**)[g]	−1.024	−0.383 (**−30.7%**)[g]	−0.511	0.127	4.009
$(O_2N)_2C{=}C(NH_2)\text{-}H_2N{\cdots}Cp_2ZrCH_3^+$	C26-N30	1.421	0.298 (**−13.4%**)[g]	−0.991	−0.372 (**−32.6%**)[g]	−0.496	0.124	3.995
$(O_2N)_2C{=}C(NH_2)\text{-}H_2N{\cdots}Cp_2HfCH_3^+$	C26-N30	1.420	0.299 (**−13.1%**)[g]	−0.994	−0.373 (**−32.5%**)[g]	−0.497	0.124	3.995

[a]Bond distance (Å), [b]Electron density (e Å^{-3}), [c]Laplacian of the electron density (e Å^{-5}), [d]Total electron energy density ($Hartree$ Å^{-3}), [e]Potential electron energy density ($V(\mathbf{r}_B)$, $Hartree$ Å^{-3}), [f]Kinetic electron energy density ($G(\mathbf{r}_B)$, $Hartree$ Å^{-3}). The vector $\mathbf{r}_B$ locates the position of the critical point.

their formation. This result is also in agreement with the increase in C-NO_2 bond length by about 1.0%, leading to its weakening. This suggests that the NH_2 group has a stabilising effect on the C-NO_2 bond in the isolated FOX-7 molecule. One possible explanation is that by donating its lone pair to one of the oxygen atoms, the nitrogen atom in NO_2 carries a positive charge. Therefore, the molecule will attempt to stabilise its positive charge through the resonance (lone pair of N) and inductive (electronegativity difference between *N* and C in C-NH_2) effects caused by NH_2. These two effects lead to an increase in the electron density along the C-NO_2 bond, resulting the increased molecular stability. Moreover, the intermolecular interaction in $(O_2N)_2C{=}C(NH_2)\text{-}H_2\mathbf{N}{\cdots}Cp_2\mathbf{M}CH_3^+$ significantly weakens the C-NH_2 bond, as evidenced by the decrease in $\rho(\mathbf{r_B})$ (from 11.1 to 13.4%) and $H(\mathbf{r_B})$ (from 30.7 to 32.6%) after the complexes formation. MMC seems to act specifically on the C-NO_2 bond by strengthening it, which is expected from a neutraliser.

3.3. EDA-NOCV analysis

The EDA-NOCV results are summarised in Table 3. All these energy terms are expressed as the difference between the two molecular interacting fragments before and after bond formation. The percentages in parentheses emphasise the contribution to the stabilising interactions (attractive terms), and the numbers in bold indicate the largest values for each complex.

From Table 3, the interaction energies are significantly more stable in complexes $(H_2N)_2C{=}C(NO_2)\text{-}(O)N\mathbf{O}{\cdots}Cp_2\mathbf{M}CH_3^+$ in comparison to $(O_2N)_2C{=}C(NH_2)\text{-}H_2\mathbf{N}{\cdots}Cp_2\mathbf{M}CH_3^+$, their difference in interaction energies is about 21.8 kcal/mol on average. These findings emphasise that the interaction between the metal centre of MMC and the oxygen atom is more stabilising than the one with the nitrogen atom. Besides, whatever the atom (oxygen or nitrogen) interacting with M = {Ti, Zr, Hf}, it appears that the Hf-based complexes exhibit the best structural stability. The most stable complex is $(H_2N)_2C{=}C(NO_2)\text{-}(O)N\mathbf{O}{\cdots}Cp_2\mathbf{Hf}CH_3^+$ with a value of −54.26 kcal/mol, and the least stable complex is $(O_2N)_2C{=}C(NH_2)\text{-}H_2\mathbf{N}{\cdots}Cp_2\mathbf{Ti}CH_3^+$ with a value of −24.96 kcal/mol.

In general terms, the magnitudes of the electrostatic (ΔE_{elstat}) and orbital (ΔE_{orb}) interactions are smaller for the complex $(O_2N)_2C{=}C(NH_2)\text{-}H_2\mathbf{N}{\cdots}Cp_2\mathbf{M}CH_3^+$ than for $(H_2N)_2C{=}C(NO_2)\text{-}(O)N\mathbf{O}{\cdots}Cp_2\mathbf{M}CH_3^+$, in such a way that the covalent interactions and electrostatic attraction in $(H_2N)_2C{=}C(NO_2)\text{-}(O)N\mathbf{O}{\cdots}Cp_2\mathbf{M}CH_3^+$ are stronger than they are in the set of complexes $(O_2N)_2C{=}C(NH_2)\text{-}H_2\mathbf{N}{\cdots}Cp_2\mathbf{M}CH_3^+$.

The orbital (covalent character) terms are predominant and contribute 40.1–41.3% to the total attractive interactions in $(O_2N)_2C{=}C(NH_2)\text{-}H_2\mathbf{N}{\cdots}Cp_2\mathbf{M}CH_3^+$ complexes, while the electrostatic and dispersion terms contribute 36.2–39.9% and 18.7–23.6%, respectively. The large orbital contributions denote the covalent character of the N ⋯ M = {Ti, Zr, Hf} bond since this interaction leads to an accumulation of negative charge in the bonding region. In contrast, the electrostatic terms are more dominant in complexes of type $(H_2N)_2C{=}C(NO_2)\text{-}(O)N\mathbf{O}{\cdots}Cp_2\mathbf{M}CH_3^+$. The largest electrostatic component (−55.04 kcal/mol) is observed for the $(H_2N)_2C{=}C(NO_2)\text{-}(O)N\mathbf{O}{\cdots}Cp_2\mathbf{Hf}CH_3^+$ complex, contributing 52.2% to the total attractive interactions. The dispersion interactions are more prominent in complexes of type $(O_2N)_2C{=}C(NH_2)\text{-}H_2\mathbf{N}{\cdots}Cp_2\mathbf{M}CH_3^+$, this component seems to

Table 3
Results of the EDA-NOCV calculations at the DFT/revPBE-D3(BJ)/TZ2P level of theory[a]. All the values are in kcal/mol.

Complex	ΔE_{Pauli}	ΔE_{orb}	ΔE_{elstat}	ΔE_{disp}	ΔE_{int} [b]
$(O_2N)_2C{=}C(NH_2)\text{-}H_2N{\cdots}Cp_2TiCH_3^+$	45.88	−28.44 (40.14%)	−25.67 (36.23%)	**−16.73** (23.61%)	−24.96
$(O_2N)_2C{=}C(NH_2)\text{-}H_2N{\cdots}Cp_2ZrCH_3^+$	40.47	−28.14 (40.85%)	−25.55 (37.09%)	−15.18 (22.04%)	−28.40
$(O_2N)_2C{=}C(NH_2)\text{-}H_2N{\cdots}Cp_2HfCH_3^+$	**46.58**	**−32.19** (41.38%)	**−31.04** (39.90%)	−14.55 (18.70%)	**−31.19**
$(H_2N)_2C{=}C(NO_2)\text{-}(O)NO{\cdots}Cp_2TiCH_3^+$	**52.06**	−36.71 (37.63%)	−50.07 (51.33%)	**−10.76** (11.03%)	−45.48
$(H_2N)_2C{=}C(NO_2)\text{-}(O)NO{\cdots}Cp_2ZrCH_3^+$	45.10	−37.40 (39.13%)	−49.40 (51.68%)	−8.77 (9.17%)	−50.47
$(H_2N)_2C{=}C(NO_2)\text{-}(O)NO{\cdots}Cp_2HfCH_3^+$	51.12	**−41.58** (39.45%)	**−55.04** (52.23%)	−8.76 (8.31%)	**−54.26**

[a] The EDA-NOCV method was conducted with a single point calculation at the DFT/revPBE-D3(BJ)/TZ2P level of theory from the fully optimised molecular structures using the CAM-B3LYP density functional. [b] The interaction energy is calculated according to: $\Delta E_{int} = \Delta E_{Pauli} + \Delta E_{orb} + \Delta E_{elstat} + \Delta E_{disp}$. The percentages in parentheses indicate the contribution to the stabilising interactions (attractive terms). The numbers in bold highlight the largest values for each energetic term in $(H_2N)_2C{=}C(NO_2)\text{-}(O)NO{\cdots}Cp_2MCH_3^+$ and $(O_2N)_2C{=}C(NH_2)\text{-}H_2N{\cdots}Cp_2MCH_3^+$.

play a major role in stabilising these complexes. The largest value (−16.73 kcal/mol) is achieved for the $(O_2N)_2C{=}C(NH_2)\text{-}H_2\mathbf{N}{\cdots}Cp_2\mathbf{Ti}CH_3^+$ complex, providing 23.61% of the total attractive interactions. The contribution of dispersion interactions is relatively small in complexes of type $(H_2N)_2C{=}C(NO_2)\text{-}(O)N\mathbf{O}{\cdots}Cp_2\mathbf{M}CH_3^+$, varying narrowly from 8.3 to 11.0%. The Pauli repulsion between like-spin electrons plays a destabilising role and naturally leads to a decrease in electron density in the bonding region.

The $(H_2N)_2C{=}C(NO_2)\text{-}(O)N\mathbf{O}{\cdots}Cp_2\mathbf{Ti}CH_3^+$ and $(H_2N)_2C{=}C(NO_2)\text{-}(O)N\mathbf{O}{\cdots}Cp_2\mathbf{Hf}CH_3^+$ complexes exhibit this effect more significantly, with values reaching up to 52.06 and 51.12 kcal/mol, respectively. However, this destabilising energy is compensated by the electrostatic interaction as their magnitudes are fairly similar. Based on the aforementioned contributions, it may be concluded that the $\{O,N\} = X \cdots M = \{Ti, Zr, Hf\}$ bond is more covalent in $(O_2N)_2C{=}C(NH_2)\text{-}H_2\mathbf{N}{\cdots}Cp_2\mathbf{M}CH_3^+$, whereas it is more ionic in $(H_2N)_2C{=}C(NO_2)\text{-}(O)N\mathbf{O}{\cdots}Cp_2\mathbf{M}CH_3^+$.

Subsequently, the density deformation due to the orbital interaction described by the first two NOCV orbitals have been analysed in detail. Visualising deformation densities helps to understand which interaction plays primary and secondary roles between the interacting species. The isosurface maps of $\Delta\rho(\mathbf{r})^{(1)}$ and $\Delta\rho(\mathbf{r})^{(2)}$ associated to the σ-donation and π-backdonation of the first two NOCV pairs are shown in Figs. 5 and 6. The orbital interaction energy contributions from the first two NOCV pairs are also indicated.

The deformation density map reveals the change in electron density distribution during the interaction between the two molecular fragments. The direction of the charge flow is highlighted by arrows (from red to blue). The red and blue isosurfaces show the regions of concentration and depletion of electron density caused by the orbital interaction due to the first two NOCV pairs, respectively.

From these Figures, it is readily apparent that the overall effect of the interaction between FOX-7 and MMC induces an increase in electron density in the bonding region. The breakdown of the orbital term enables quantifying the donation and backdonation strength of MMC in each complex, which can be classified according to their donor or acceptor properties.

The σ-donations from occupied orbitals of nitrogen ($N \longrightarrow Cp_2MCH_3^+$) are significantly stronger than π-backdonation from $Cp_2MCH_3^+$ to N ($Cp_2MCH_3^+ \longrightarrow N$) in complexes of type $(O_2N)_2C{=}C(NH_2)\text{-}H_2\mathbf{N}{\cdots}Cp_2\mathbf{M}CH_3^+$. This result is expected since NH_2 is an electron-rich species that tends to donate electrons to the electron-deficient species $M = \{Ti, Zr, Hf\}$ that tends to accept electrons through its unoccupied $(n-1)d$ orbital. The charge transfer ($N \longrightarrow Cp_2MCH_3^+$) occurs in a fairly narrow range, from |0.41| to |0.44|. In these complexes, the effect of backdonation is very small, its contribution is almost negligible since the energy of the second NOCV pair is ∼ −1.0 kcal/mol. The situation is different concerning the $(H_2N)_2C{=}C(NO_2)\text{-}(O)N\mathbf{O}{\cdots}Cp_2\mathbf{M}CH_3^+$ complexes (see Fig. 5), where both charge transfers correspond to the σ-donation. The second NOCV contributions to deformation density show that the σ-component also corresponds to the donation from the lone electron pair of oxygen into a vacant orbital of $M=\{Ti, Zr, Hf\}$. The oxygen atom acts as a Lewis base donating its lone electron pair to the metal centre. The two charge transfers reinforce each other, resulting in increased stability for $(H_2N)_2C{=}C(NO_2)\text{-}(O)N\mathbf{O}{\cdots}Cp_2\mathbf{M}CH_3^+$. This seems to strengthen the $(H_2N)_2C{=}C(NO_2)\text{-}(O)N\mathbf{O}{\cdots}M=\{Ti, Zr, Hf\}$ bond, which may explain the high stability of $(H_2N)_2C{=}C(NO_2)\text{-}(O)N\mathbf{O}{\cdots}Cp_2\mathbf{M}CH_3^+$ compared to $(O_2N)_2C{=}C(NH_2)\text{-}H_2\mathbf{N}{\cdots}Cp_2\mathbf{M}CH_3^+$. The interaction between the $(H_2N)_2C{=}C(NO_2)\text{-}(O)N\mathbf{O}$ ligand and the $M=\{Ti, Zr, Hf\}$ moiety is dominated by the σ forward donation, indicating the σ-donating ability of this ligand. The strong σ-donor achieves good overlap with the metal orbital, and the resulting interaction is low-energy.

4. Conclusion

The local chemical reactivity of FOX-7 towards nucleophilic and electrophilic reagents was characterised through a quantitative analysis of the ESP on the molecular surface. As expected, significant negative ESP values are found over the nitro groups, while positive ESP values are located above the C-NO_2 bonds indicating a decrease in electron density due to the high electron-withdrawing effect of NO_2 group. The central regions are characterised by large positive ESP, typical of energetic molecules.

Results derived from QTAIM showed that the C-NO_2 bonds are influenced by the $O \cdots M = \{Ti, Zr, Hf\}$ bonding. Indeed, the formation of complexes of type $(H_2N)_2C{=}C(NO_2)\text{-}(O)N\mathbf{O}{\cdots}Cp_2\mathbf{M}CH_3^+$ strengthens the C-NO_2 bond, which provides additional stability to the molecular structure of FOX-7. In addition, the shorter distances of C-NO_2 observed in $(H_2N)_2C{=}C(NO_2)\text{-}(O)N\mathbf{O}{\cdots}Cp_2\mathbf{M}CH_3^+$ confirm the strengthening of these bonds after interaction with MMC. Furthermore, the interaction O⋯M rules the complex formation when a nitro group interacts with MMC, which is reactive through its transition metal.

The interaction energies calculated by EDA-NOCV revealed that the $(H_2N)_2C{=}C(NO_2)\text{-}(O)N\mathbf{O}{\cdots}Cp_2\mathbf{M}CH_3^+$ complexes are significantly more structurally stable (by about 21.8 kcal/mol) than the $(O_2N)_2C{=}C(NH_2)\text{-}H_2\mathbf{N}{\cdots}Cp_2\mathbf{M}CH_3^+$ complexes. The electrostatic terms varying from 51.1 to 52.2% are clearly more dominant in complexes of type $(H_2N)_2C{=}C(NO_2)\text{-}(O)N\mathbf{O}{\cdots}Cp_2\mathbf{M}CH_3^+$ compared to the set of complexes like $(O_2N)_2C{=}C(NH_2)\text{-}H_2\mathbf{N}{\cdots}Cp_2\mathbf{M}CH_3^+$ (from 36.2 to 39.9%). In contrast, the orbital terms are slightly predominant in complexes of type $(O_2N)_2C{=}C(NH_2)\text{-}H_2\mathbf{N}{\cdots}Cp_2\mathbf{M}CH_3^+$ and contribute 40.1–41.3% to the total attractive interactions. Overall, the dispersion interactions are less important compared to the other attractive terms, but are slightly higher in $(O_2N)_2C{=}C(NH_2)\text{-}H_2\mathbf{N}{\cdots}Cp_2\mathbf{M}CH_3^+$ ranging from 18.7 to 23.6%.

Based on the first NOCV pair energy, the σ-donor character is more prominent in $(O_2N)_2C{=}C(NH_2)\text{-}H_2\mathbf{N}{\cdots}Cp_2\mathbf{M}CH_3^+$ compared to $(H_2N)_2C{=}C(NO_2)\text{-}(O)N\mathbf{O}{\cdots}Cp_2\mathbf{M}CH_3^+$. This seems to strengthen the $(H_2N)_2C{=}C(NO_2)\text{-}(O)N\mathbf{O}{\cdots}M=\{Ti, Zr, Hf\}$ bond, which may explain the high stability of $(H_2N)_2C{=}C(NO_2)\text{-}(O)N\mathbf{O}{\cdots}Cp_2\mathbf{M}CH_3^+$ compared to $(O_2N)_2C{=}C(NH_2)\text{-}H_2\mathbf{N}{\cdots}Cp_2\mathbf{M}CH_3^+$.

This study allows us to further understand the effect of these intermolecular interactions on the stabilisation of such bonds, for designing less sensitive energetic molecules allowing more secure handling. In

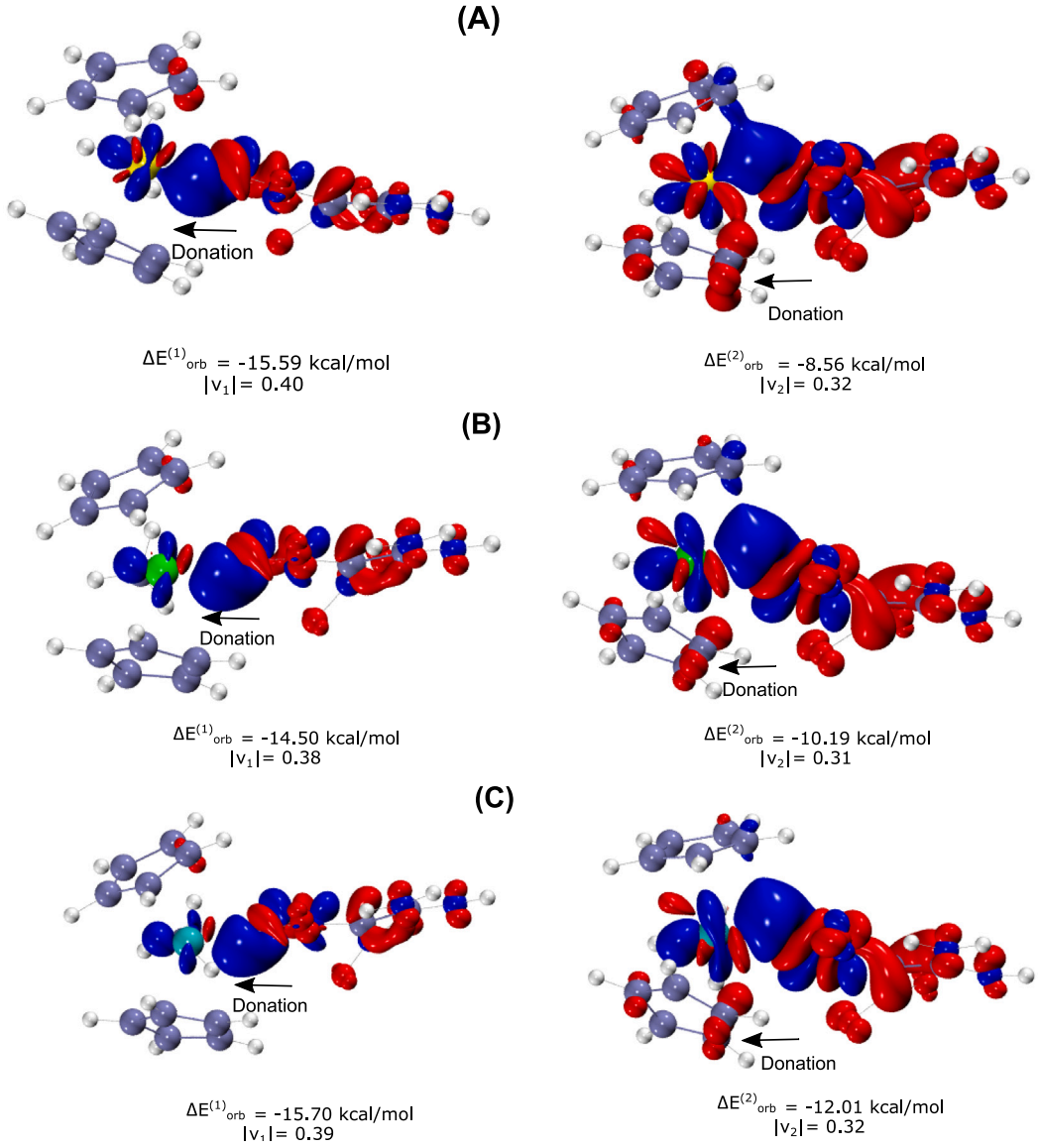


Fig. 5. ETS-NOCV deformation densities in complexes $(H_2N)_2C{=}C(NO_2)\text{-}(O)N\mathbf{O}\cdots Cp_2\mathbf{M}CH_3^+$. (A):$(H_2N)_2C{=}C(NO_2)\text{-}(O)N\mathbf{O}\cdots Cp_2\mathbf{Ti}CH_3^+$, (B):$(H_2N)_2C{=}C(NO_2)\text{-}(O)N\mathbf{O}\cdots Cp_2\mathbf{Zr}CH_3^+$ and (C):$(H_2N)_2C{=}C(NO_2)\text{-}(O)N\mathbf{O}\cdots Cp_2\mathbf{Hf}CH_3^+$. The red and blue contours correspond to accumulation and depletion of electron density, respectively. Direction of the negative charge flow: red→blue. The eigenvalues $|\nu|$ yield the extent of the charge flow. The deformation densities were plotted with the contour values 0.002 a.u. for $\Delta\rho(\mathbf{r})^{(1)}$ and 0.0006 a.u. for $\Delta\rho(\mathbf{r})^{(2)}$. (For interpretation of the references to colour in this figure legend, the reader is referred to the web version of this article.)

addition, if we cannot prevent the explosive behaviour of molecules like FOX-7, at least we can diminish their sensitivity for safer handling through the formation of these types of complexes with metallocene methyl cations.

Declaration of competing interest

The authors declare that they have no known competing financial interests or personal relationships that could have appeared to influence the work reported in this paper.

Data availability

Data will be made available on request.

Acknowledgements

J.I. Martínez-Araya acknowledges the financial support provided by the former Fondo Nacional de Desarrollo Científico y Tecnológico, FONDECYT, Chile grant No 1181504 from Agencia Nacional de Investigación *y* Desarrollo (Chile). N. Bachir and S. Kenouche acknowledge the financial support provided by the Ministry of Higher Education and Scientific Research (Algeria), PRFU project-code: B00L01UN070120220004. The authors wish to thank Professor N. Nebbache for technical support in collaboration with Professor H. Chermette (Institute of Analytical Sciences, UMR 5280, Lyon).

Dedication

The present work is dedicated to the memory of Dr. Peter Politzer (1937, Prague, Czechoslovakia – 2022, New Orleans, USA) who paved the way for studying molecular interactions through the rutinary use of the electrostatic potential based on quantum chemical calculations.

Appendix A. Supplementary data

Supplementary material related to this article can be found online at https://doi.org/10.1016/j.jmgm.2023.108645.

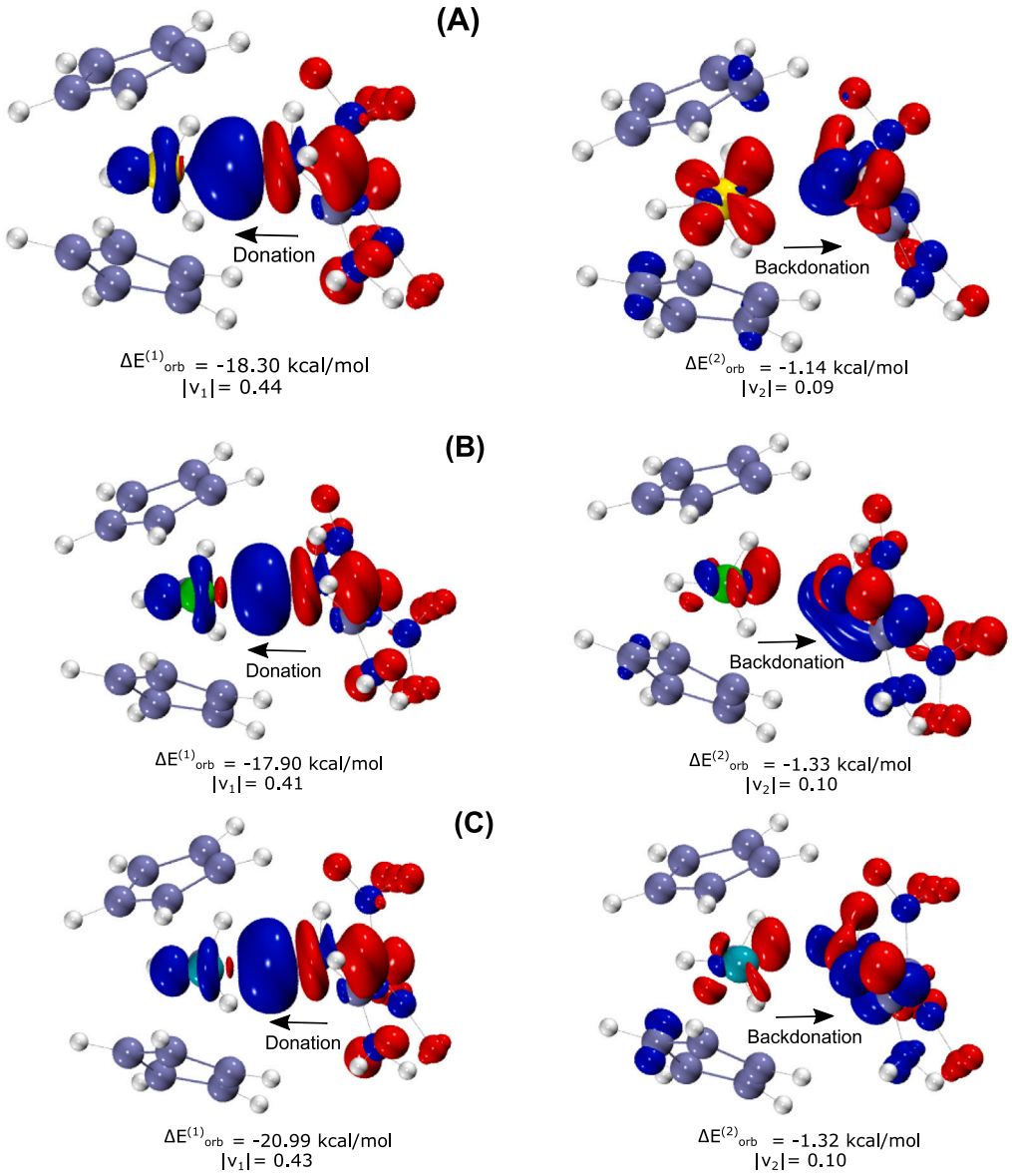


Fig. 6. ETS-NOCV deformation densities in complexes $(O_2N)_2C{=}C(NH_2)\text{-}H_2\mathbf{N}\cdots Cp_2\mathbf{M}CH_3^+$. (A):$(O_2N)_2C{=}C(NH_2)\text{-}H_2\mathbf{N}\cdots Cp_2\mathbf{Ti}CH_3^+$, (B):$(O_2N)_2C{=}C(NH_2)\text{-}H_2\mathbf{N}\cdots Cp_2\mathbf{Zr}CH_3^+$ and (C):$(O_2N)_2C{=}C(NH_2)\text{-}H_2\mathbf{N}\cdots Cp_2\mathbf{Hf}CH_3^+$. The red and blue contours correspond to accumulation and depletion of electron density, respectively. Direction of the negative charge flow: red→blue. The eigenvalues $|\nu|$ yield the extent of the charge flow. The deformation densities were plotted with the contour values 0.002 a.u. for $\Delta\rho(\mathbf{r})^{(1)}$ and 0.0006 a.u. for $\Delta\rho(\mathbf{r})^{(2)}$. (For interpretation of the references to colour in this figure legend, the reader is referred to the web version of this article.)

References

[1] Roman V. Tsyshevsky, Onise Sharia, Maija M. Kuklja, Thermal decomposition mechanisms of nitroesters: Ab initio modeling of pentaerythritol tetranitrate, J. Phys. Chem. C 117 (35) (2013) 18144–18153.

[2] Roman V. Tsyshevsky, Onise Sharia, Maija M. Kuklja, Molecular theory of detonation initiation: insight from first principles modeling of the decomposition mechanisms of organic nitro energetic materials, Molecules 21 (2) (2016) 236.

[3] Ying Xiong, Kai Zhong, Chao-yang Zhang, Trigger linkage mechanism: Two or multiple steps initiate the spontaneous decay of energetic materials, Energetic Mater. Front. 3 (1) (2022) 38–46.

[4] Thomas B. Brill, Kenneth J. James, Kinetics and mechanisms of thermal decomposition of nitroaromatic explosives, Chem. Rev. 93 (8) (1993) 2667–2692.

[5] Peter Politzer, Jane S. Murray, C–NO_2 dissociation energies and surface electrostatic potential maxima in relation to the impact sensitivities of some nitroheterocyclic molecules, Mol. Phys. 86 (2) (1995) 251–255.

[6] Peter Politzer, Jane S. Murray, Relationships between dissociation energies and electrostatic potentials of C–NO_2 bonds: Applications to impact sensitivities, J. Mol. Struct. 376 (1–3) (1996) 419–424.

[7] Maija M. Kuklja, Eugene V. Stefanovich, A Barry Kunz, An excitonic mechanism of detonation initiation in explosives, J. Chem. Phys. 112 (7) (2000) 3417–3423.

[8] Svatopluk Zeman, Sensitivities of high energy compounds, High Energy Density Mater. (2007) 195–271.

[9] Jane S. Murray, Monica C. Concha, Peter Politzer, Links between surface electrostatic potentials of energetic molecules, impact sensitivities and C–NO_2/N–NO_2 bond dissociation energies, Mol. Phys. 107 (1) (2009) 89–97.

[10] M.J. Kamlet, H.G. Adolph, The relationship of impact sensitivity with structure of organic high explosives. ii. Polynitroaromatic explosives, Propellants, Explos., Pyrotech. 4 (2) (1979) 30–34.

[11] Peter Politzer, Jane S. Murray, Detonation performance and sensitivity: A quest for balance, in: Advances in Quantum Chemistry, vol. 69, Elsevier, 2014, pp. 1–30.

[12] Scott A. Shackelford, Role of Thermochemical Decomposition in Energetic Material Initiation Sensitivity and Explosive Performance, Technical report, AIR FORCE RESEARCH LAB EDWARDS AFB CA, 2007.

[13] Jacqueline Akhavan, The chemistry of explosives, R. Soc. Chem. (2011).

[14] Laurence E. Fried, M. Riad Manaa, Philip F. Pagoria, Randall L. Simpson, Design and synthesis of energetic materials, Annu. Rev. Mater. Res. 31 (1) (2001) 291–321.

[15] Sury Iyer, Norman Slagg, Molecular Aspects in Energetic Materials, VCH Publishers, New York, 1988.

[16] Peter Politzer, Pat Lane, Jane S. Murray, Electrostatic potentials, intralattice attractive forces and crystal densities of nitrogen-rich C, H, N, O salts, Crystals 6 (1) (2016) 7.

[17] Anna V. Kimmel, Peter V. Sushko, Alexander L. Shluger, Maija M. Kuklja, Effect of charged and excited states on the decomposition of 1, 1-diamino-2, 2-dinitroethylene molecules, J. Chem. Phys. 126 (23) (2007) 234711.

[18] Jun Tao, Xiaofeng Wang, Theoretical investigation on the interaction mechanism of FOX-7/AP mixed crystals, Mol. Simul. 46 (2) (2020) 155–161.

[19] Betsy M. Rice, Jennifer J. Hare, A quantum mechanical investigation of the relation between impact sensitivity and the charge distribution in energetic molecules, J. Phys. Chem. A 106 (9) (2002) 1770–1783.

[20] Joaquín O. Singh, Jorge D. Anunziata, Juana J. Silber, N–π electron donor–acceptor complexes. ii. Aliphatic amines with dinitrobenzenes, Canad. J. Chem. 63 (4) (1985) 903–907.

[21] Divyakant L. Patel, James Dillon, Noel Wright, In-situ landmine neutralization using chemicals to initiate low order burning of main charge, 2006.

[22] Nikolai V. Latypov, Jan Bergman, Abraham Langlet, Ulf Wellmar, Ulf Bemm, Synthesis and reactions of 1, 1-diamino-2, 2-dinitroethylene, Tetrahedron 54 (38) (1998) 11525–11536.

[23] Yu Zhang, Qian Sun, Kangzhen Xu, Jirong Song, Fengqi Zhao, Review on the reactivity of 1, 1-diamino-2, 2-dinitroethylene (fox-7), Propellants, Explos., Pyrotech. 41 (1) (2016) 35–52.

[24] Dan C. Sorescu, Jerry A. Boatz, Donald L. Thompson, Classical and quantum-mechanical studies of crystalline FOX-7 (1, 1-diamino-2, 2-dinitroethylene), J. Phys. Chem. A 105 (20) (2001) 5010–5021.

[25] Xue-Hai Ju, He-Ming Xiao, Qi-Ying Xia, A density functional theory investigation of 1, 1-diamino-2, 2-dinitroethylene dimers and crystal, J. Chem. Phys. 119 (19) (2003) 10247–10255.

[26] Jijun Zhao, Hong Liu, High-pressure behavior of crystalline FOX-7 by density functional theory calculations, Comput. Mater. Sci. 42 (4) (2008) 698–703.

[27] Jorge M. del Campo, Jorge Ignacio Martínez-Araya, Possible use of group 4 metallocene methyl cations as potential neutralizers for FOX-7, Propellants, Explos., Pyrotech. 39 (6) (2014) 890–896.

[28] Steven Hunter, Paul L. Coster, Alistair J. Davidson, David I.A. Millar, Stewart F. Parker, William G. Marshall, Ronald I. Smith, Carole A. Morrison, Colin R. Pulham, High-pressure experimental and DFT-D structural studies of the energetic material FOX-7, J. Phys. Chem. C 119 (5) (2015) 2322–2334.

[29] Zbigniew A. Dreger, Yuchuan Tao, Yogendra M. Gupta, Phase diagram and decomposition of 1, 1-diamino-2, 2-dinitroethene single crystals at high pressures and temperatures, J. Phys. Chem. C 120 (20) (2016) 11092–11098.

[30] Yongxing Tang, Wei Huang, Gregory H. Imler, Damon A. Parrish, Jeanne M. Shreeve, Enforced planar FOX-7-like molecules: A strategy for thermally stable and insensitive π-conjugated energetic materials, J. Am. Chem. Soc. 142 (15) (2020) 7153–7160.

[31] Haixiang Gao, M. Shreeve Jean'ne, Recent progress in taming FOX-7 (1, 1-diamino-2, 2-dinitroethene), RSC Advances 6 (61) (2016) 56271–56277.

[32] Yang Liu, Feng Li, Huai Sun, Thermal decomposition of FOX-7 studied by ab initio molecular dynamics simulations, in: Guosen Yan, Springer, 2015, pp. 165–175.

[33] Yingzhe Liu, Yiding Ma, Tao Yu, Weipeng Lai, Wangjun Guo, Zhongxue Ge, Zhinan Ma, Structural rearrangement of energetic materials under an external electric field: A case study of nitromethane, J. Phys. Chem. A 122 (8) (2018) 2129–2134.

[34] Ludmila Simkova, Frantisek Liska, Jiri Ludvik, 2, 2-dinitroethene-1, 1-diamine, Curr. Org. Chem. 15 (17) (2011) 2983–2995.

[35] P. Cossee. Ziegler-natta catalysis i, Mechanism of polymerisation of α-olefins with Ziegler–Natta catalysts, J. Catal. 3 (1) (1964) 80–88.

[36] E.J. Arlman, Ziegler–Natta catalysis ii. Surface structure of layer-lattice transition metal chlorides, J. Catal. 3 (1) (1964) 89–98.

[37] Nassima Bachir, Samir Kenouche, Jorge I. Martínez-Araya, Theoretical investigation of the effect of O···M={Ti, Zr, Hf} interactions on the sensitivity of energetic N-nitro compounds, J. Mol. Graphics Model. 118 (2023) 108341.

[38] Waldemar A. Trzciński, Stanisław Cudziło, Zbigniew Chyłek, Leszek Szymańczyk, Detonation properties of 1, 1-diamino-2, 2-dinitroethene (DADNE), J. Hazard. Mater. 157 (2–3) (2008) 605–612.

[39] Qiong Wu, Weihua Zhu, Heming Xiao, Dft study on crystalline 1, 1-diamino-2, 2-dintroethylene under high pressures, J. Mol. Model. 19 (9) (2013) 4039–4047.

[40] Peter Politzer, Monica C. Concha, M. Edward Grice, Jane S. Murray, Pat Lane, Computational investigation of the structures and relative stabilities of amino/nitro derivatives of ethylene, J. Mol. Struct.: THEOCHEM 452 (1–3) (1998) 75–83.

[41] Yu-Ran Luo, Comprehensive HandBook of Chemical Bond Energies, CRC Press, 2007.

[42] Miroslav Pospíšil, Pavel Vávra, Monica C. Concha, Jane S. Murray, Peter Politzer, Sensitivity and the available free space per molecule in the unit cell, J. Mol. Model. 17 (10) (2011) 2569–2574.

[43] Peter Politzer, Jane S. Murray, Some perspectives on sensitivity to initiation of detonation, Green Energetic Mater. (2014) 45–62.

[44] F. Matthias Bickelhaupt, Célia Fonseca Guerra, Mariusz Paweł Mitoraj, Filip Sagan, Artur Michalak, Sudip Pan, Gernot Frenking, Clarifying notes on the bonding analysis adopted by the energy decomposition analysis, Phys. Chem. Chem. Phys. (2022).

[45] Peter Politzer, Robert Parr, Some new energy formulas for atoms and molecules, J. Chem. Phys. 61 (10) (1974) 4258–4262.

[46] Peter Politzer, Jane S. Murray, The fundamental nature and role of the electrostatic potential in atoms and molecules, Theor. Chem. Accounts 108 (2002) 134–142.

[47] Peter Politzer, Atomic and molecular energies as functionals of the electrostatic potential, Theor. Chem. Accounts 111 (2004) 395–399.

[48] Jane S. Murray, Peter Politzer, The electrostatic potential: An overview, WIREs Comput. Mol. Sci. 1 (2) (2011) 153–163.

[49] Peter Politzer, Pat Lane, Jane S. Murray, Tricyclic polyazine n-oxides as proposed energetic compounds, Central Eur. J. Energetic Mater. 10 (3) (2013).

[50] Anton Hammerl, Thomas M. Klapötke, Heinrich Nöth, Markus Warchhold, Gerhard Holl, Synthesis, structure, molecular orbital and valence bond calculations for tetrazole azide, CHN_7, Propellants, Explos., Pyrotech.: Int. J. Deal. Sci. Technol. Aspects Energetic Mater. 28 (4) (2003) 165–173.

[51] Thomas M. Klapötke, Andreas Nordheider, Jörg Stierstorfer, Synthesis and reactivity of an unexpected highly sensitive 1-carboxymethyl-3-diazonio-5-nitrimino-1, 2, 4-triazole, New J. Chem. 36 (7) (2012) 1463–1468.

[52] Elif. Gökçınar, Thomas.M. Klapötke, Anthony J. Bellamy, Computational study on 2, 6-diamino-3, 5-dinitropyrazine and its 1-oxide and 1, 4-dioxide derivatives, J. Mol. Struct.: THEOCHEM 953 (1–3) (2010) 18–23.

[53] Jane S. Murray, Tore Brinck, Pat Lane, Kirn Paulsen, Peter Politzer, Statistically-based interaction indices derived from molecular surface electrostatic potentials: A general interaction properties function (gipf), J. Mol. Struct.: THEOCHEM 307 (1994) 55–64.

[54] Peter Politzer, Jorge Martinez, Jane S. Murray, Monica C. Concha, Alejandro Toro-Labbé, An electrostatic interaction correction for improved crystal density prediction, Mol. Phys. 107 (2009) 2095–2101.

[55] Peter Politzer, Jorge Martinez, Jane S. Murray, C. Monica, Concha an electrostatic correction for improved crystal density predictions of energetic ionic compounds, Mol. Phys. 108 (2010) 1391–1396.

[56] A. Luna, B. Amekraz, J.-P. Morizur, J. Tortajada, O. Mó, M. Yáñez, Reactions between guanidine and Cu^+ in the gas phase. an experimental and theoretical study, J. Phys. Chem. A 101 (33) (1997) 5931–5941.

[57] J.-L.M. Abboud, I. Alkorta, J.Z. Dávalos, J.-F. Gal, M. Herreros, P.-C. Maria, O. Mó, M.T. Molina, R. Notario, M. Yáñez, The $P_4 \cdots Li^+$ ion in the gas phase: A planetary system, J. Am. Chem. Soc. 122 (18) (2000) 4451–4454.

[58] Manuel Alcamí, Alberto Luna, Otilia Mó, Manuel Yáñez, Jeanine Tortajada, Badia Amekraz, Unimolecular reactivity of strong metal–cation complexes in the gas phase: Ethylenediamine–Cu^+, Chem. Eur. J. 10 (12) (2004) 2927–2934.

[59] Sai Manoj N.V.T. Gorantla, Kartik Chandra Mondal, Uncovering the hidden reactivity of benzyne/aryne precursors utilized under milder condition: Bonding and stability studies by EDA–NOCV analyses, J. Comput. Chem. 43 (23) (2022) 1543–1560.

[60] Kavita Devi, Sai Manoj N.V.T. Gorantla, Kartik Chandra Mondal, EDA-NOCV analysis of carbene-borylene bonded dinitrogen complexes for deeper bonding insight: A fair comparison with a metal-dinitrogen system, J. Comput. Chem. 43 (11) (2022) 757–777.

[61] Kenouche Samir, Bachir Nassima, Jorge I. Martínez-Araya, Explaining the high catalytic activity in bis (indenyl) methyl zirconium cation using combined EDA-NOCV/QTAIM approach, ChemPhysChemy 24 (2) (2023) e202200488.

[62] Sai Manoj N.V.T. Gorantla, Kartik Chandra Mondal, EDA–NOCV calculation for efficient N_2 binding to the reduced Ni_3S_8 complex: Estimation of Ni–N_2 intrinsic interaction energies, ACS Omega 6 (49) (2021) 33389–33397.

[63] Tom Ziegler, Arvi Rauk, Carbon monoxide, carbon monosulfide, molecular nitrogen, phosphorus trifluoride, and methyl isocyanide as. sigma. donors and. pi. acceptors. A theoretical study by the Hartree–Fock-Slater transition-state method, Inorg. Chem. 18 (7) (1979) 1755–1759.

[64] Tom Ziegler, Arvi Rauk, A theoretical study of the ethylene-metal bond in complexes between copper (1+), silver (1+), gold (1+), platinum (0) or platinum (2+) and ethylene, based on the Hartree–Fock-Slater transition-state method, Inorg. Chem. 18 (6) (1979) 1558–1565.

[65] Mariusz Mitoraj, Artur Michalak, Donor–acceptor properties of ligands from the natural orbitals for chemical valence, Organometallics 26 (26) (2007) 6576–6580.

[66] Mariusz Mitoraj, Artur Michalak, Applications of natural orbitals for chemical valence in a description of bonding in conjugated molecules, J. Mol. Model. 14 (8) (2008) 681–687.

[67] Gernot Frenking, F. Matthias Bickelhaupt, The eda perspective of chemical bonding. the chemical bond: fundamental aspects of chemical bonding, 2014, pp. 121–157.

[68] Lili Zhao, Markus Hermann, W.H. Schwarz, Gernot Frenking, The lewis electron-pair bonding model: Modern energy decomposition analysis, Nat. Rev. Chem. 3 (1) (2019) 48–63.

[69] Moritz von Hopffgarten, Gernot Frenking, Energy decomposition analysis, Wiley Interdiscipl. Rev.: Comput. Mol. Sci. 2 (1) (2012) 43–62.

[70] H.B. Schlegel, G.E. Scuseria, M.A. Robb, J.R. Cheeseman, G. Scalmani, V. Barone, G.A. Petersson, H. Nakatsuji, X. Li, M. Caricato, et al., Gaussian 16, Revision B. 01, Gaussian. Inc., Wallingford CT.[Google Scholar], 2016.
[71] Takeshi Yanai, David P. Tew, Nicholas C. Handy, A new hybrid exchange–correlation functional using the Coulomb-attenuating method (CAM-B3LYP), Chem. Phys. Lett. 393 (1–3) (2004) 51–57.
[72] Jeng-Da Chai, Martin Head-Gordon, Long-range corrected hybrid density functionals with damped atom–atom dispersion corrections, Phys. Chem. Chem. Phys. 10 (44) (2008) 6615–6620.
[73] Patricio Fuentealba, Heinzwerner Preuss, Hermann Stoll, Laszlo Von Szentpaly, A proper account of core-polarisation with pseudopotentials: Single valence-electron alkali compounds, Chem. Phys. Lett. 89 (5) (1982) 418–422.
[74] G. Te Velde, F. Matthias Bickelhaupt, Evert Jan Baerends, C. Fonseca Guerra, Stan J.A. van Gisbergen, Jaap G. Snijders, Tom Ziegler, Chemistry with ADF, J. Comput. Chem. 22 (9) (2001) 931–967.
[75] John P. Perdew, Kieron Burke, Matthias Ernzerhof, Generalized gradient approximation made simple, Phys. Rev. Lett. 77 (18) (1996) 3865.
[76] Stefan Grimme, Stephan Ehrlich, Lars Goerigk, Effect of the damping function in dispersion corrected density functional theory, J. Comput. Chem. 32 (7) (2011) 1456–1465.
[77] Lars Goerigk, Andreas Hansen, Christoph Bauer, Stephan Ehrlich, Asim Najibi, Stefan Grimme, A look at the density functional theory zoo with the advanced GMTKN55 database for general main group thermochemistry, kinetics and noncovalent interactions, Phys. Chem. Chem. Phys. 19 (48) (2017) 32184–32215.
[78] Erik Van Lenthe, Evert Jan Baerends, Optimised slater-type basis sets for the elements 1–118, J. Comput. Chem. 24 (9) (2003) 1142–1156.
[79] Mirko Franchini, Pierre Herman Theodoor Philipsen, Lucas Visscher, The Becke fuzzy cells integration scheme in the Amsterdam density functional program suite, J. Comput. Chem. 34 (21) (2013) 1819–1827.
[80] E. van Lenthe, Evert-Jan Baerends, Jaap G. Snijders, Relativistic regular two-component hamiltonians, J. Chem. Phys. 99 (6) (1993) 4597–4610.
[81] W. Humphrey, A. Dalke, K. Schulten, VMD: Visual molecular dynamics, J. Mol. Graph. 14 (1) (1996) 33–38.
[82] Tian Lu, Feiwu Chen, Multiwfn: A multifunctional wavefunction analyser, J. Comput. Chem. 33 (5) (2012) 580–592.
[83] R.F.W. Bader, W.H_. Henneker, Paul.E. Cade, Molecular charge distributions and chemical binding, J. Chem. Phys. 46 (9) (1967) 3341–3363.
[84] Peter Politzer, Jane S. Murray, Jorge M. Seminario, Pat Lane, M. Edward Grice, Monica C. Concha, Computational characterization of energetic materials, J. Mol. Struct.: THEOCHEM 573 (1–3) (2001) 1–10.
[85] Richard F.W. Bader, Hanno Essén, The characterization of atomic interactions, J. Chem. Phys. 80 (5) (1984) 1943–1960.
[86] Richard F.W. Bader, Preston J. MacDougall, Toward a theory of chemical reactivity based on the charge density, J. Am. Chem. Soc. 107 (24) (1985) 6788–6795.
[87] Richard F.W. Bader, A bond path: A universal indicator of bonded interactions, J. Phys. Chem. A 102 (37) (1998) 7314–7323.
[88] Richard F.W. Bader, Pauli repulsions exist only in the eye of the beholder, Chem. Eur. J. 12 (10) (2006) 2896–2901.
[89] Zhaoxu Wang, Yi Liu, Baishu Zheng, Fengxiang Zhou, Yinchun Jiao, Yuan Liu, XunLei Ding, Tian Lu, A theoretical investigation on Cu/Ag/Au bonding in $XH_2P\cdots MY$ (X=H, CH_3, F, CN, NO_2; M=Cu, Ag, Au; Y=F, Cl, Br, I) complexes, J. Chem. Phys. 148 (19) (2018) 194106.
[90] Baishu Zheng, Yi Liu, Zhaoxu Wang, Fengxiang Zhou, Yuan Liu, XunLei Ding, Tian Lu, Regium bonds formed by MX (M=Cu, Ag, Au; X=F, Cl, Br) with phosphine-oxide/phosphinous acid: Comparisons between oxygen-shared and phosphine-shared complexes, Mol. Phys. 117 (18) (2019) 2443–2455.
[91] Samir Kenouche, Jorge I Martínez-Araya, A combined QTAIM/IRI topological analysis of the effect of axial/equatorial positions of NH_2 and CN substituents in the $[(PY_5Me_2)\ MoO]^+$ complex, J. Mol. Graphics Model. 116 (2022) 108273.
[92] Enrique Espinosa, Ibon Alkorta, José Elguero, Elies Molins, From weak to strong interactions: A comprehensive analysis of the topological and energetic properties of the electron density distribution involving X–H···F–Y systems, J. Chem. Phys. 117 (12) (2002) 5529–5542.
[93] Ignacy Cukrowski, Jurgens H. de Lange, Mariusz Mitoraj, Physical nature of interactions in Zn^{II} complexes with 2, 2′-bipyridyl: Quantum theory of atoms in molecules (QTAIM), interacting quantum atoms (IQA), noncovalent interactions (NCI), and extended transition state coupled with natural orbitals for chemical valence (ETS-NOCV) comparative studies, J. Phys. Chem. A 118 (3) (2014) 623–637.